Available online at www.sciencedirect.com
ScienceDirect
Journal of Membrane Science 281 (2006) 228–238
journal of MEMBRANE SCIENCE
www.elsevier.com/locate/memsci

Nanocomposite MFI-alumina membranes via pore-plugging synthesis
Preparation and morphological characterisation

S. Miachon*, E. Landrivon, M. Aouine, Y. Sun, I. Kumakiri, Y. Li, O. Pachtová Prokopová, N. Guilhaume, A. Giroir-Fendler[1], H. Mozzanega, J.-A. Dalmon

Institut de Recherches sur la Catalyse, CNRS, 2, Av. A. Einstein, 69629 Villeurbanne Cedex, France

Received 7 February 2006; received in revised form 16 March 2006; accepted 26 March 2006
Available online 25 April 2006

Abstract

A specific synthesis protocol, based on zeolite crystallisation within the pores of a host support, the pore-plugging method, has been designed and optimised. A composite membrane has been obtained and its quality evaluated using the separation of adsorbing and non-adsorbing gas mixture.

A series of parameters were studied, including the pore size of the support, the composition of the precursor solution and the hydrothermal synthesis temperature program. Accordingly, the membrane quality showed large variations.

The material structure was characterised using scanning and transmission electron microscopies. These observations showed a composite organization at the support pore scale, with an architecture very different from conventional supported zeolite films.

The final optimisation of the synthesis conditions concluded to a precursor solution containing 2 mol/l of silica, 0.9 mol/l of TPAOH, and the use of an interrupted hydrothermal temperature program, among other parameters. Thanks to this optimisation process, an average increase of one order of magnitude in the separative performance was obtained.

Keywords: MFI zeolite; Membrane; Nanocomposite; Pore-plugging; Transmission electron microscopy

---

1. Introduction

Inorganic porous membranes, beside their current commercial applications in liquid separation, have been recently implemented at the industrial scale for pervaporation processes [1] and are widely studied at the lab level, for gas separation. The future of gas separation inorganic porous membranes will be based on their selectivity, permeability and stability characteristics. Moreover, the development of such commercial applications will depend on the availability of high quality, defect-free membranes, preferentially synthesized through simple protocols leading to cost-effective processes [2].

Due to their defined crystal structure, microporous architecture, thermal and chemical stability, zeolite materials are well adapted to make molecular sieving membranes. Moreover, they offer a range of pore size and tuned adsorption properties that can be selected or adapted (ionic substitution and exchange) according to the targeted separation.

The very first paper using the word zeolitic membranes can be traced back to 1939 [3]. The number of papers increased rapidly after 1990, and more than 3000 research papers and patents have been published, including several reviews [4–15]. This continuous research activity shows that the preparation of high quality zeolite membrane is a difficult task. The challenge is to prepare realistic membrane areas whose properties depend only on the intrinsic capabilities of the zeolite. In fact, the membrane performance is determined by the quality of the zeolite coating on the support, whose thickness must be as low as possible to favour high permeances. Moreover, beside defects, the number and nature of crystal boundaries may also influence permeation and separation properties [10,16,17].

The small pores of MFI zeolite membranes, about 0.5 nm, make them suitable for gas molecules separation. Therefore, this type of material has been widely studied, and showed most of the promising results that have been published in gas separation [18].

---

* Corresponding author. Tel.: +33 472445384.
E-mail address: sylvain.miachon@catalyse.cnrs.fr (S. Miachon).

[1] Present address: Laboratoire d'Application de la Chimie à l'Environnement, Université Claude Bernard Lyon 1, 43, Bd. du 11 novembre 1918, 69100 Villeurbanne, France.

0376-7388/$ – see front matter © 2006 Elsevier B.V. All rights reserved.
doi:10.1016/j.memsci.2006.03.036

Most of the membranes are based on a porous support that ensures mechanical resistance and allows a thin zeolite separative top-layer formation. Several strategies have been developed to achieve the preparation of such zeolite layers [10]. Among them, three are frequently used:

- The first one is a one-step process during which both nucleation and growth of the zeolite material take place in presence of the support. In this method, also called "In-situ crystallization" [19], the bare porous support is put in contact with the zeolite precursors and submitted to hydrothermal synthesis conditions. This simple strategy presents however some drawbacks. As a matter of fact, the zeolite layer should be formed from nuclei that appear during the hydrothermal treatment. Their number and distribution homogeneity on the support depend on different parameters, such as the local support surface properties, that are difficult to control. Moreover, the nuclei formation competes with the crystal growth process, which may limit the nuclei density due to mass-transfer limitations towards the support. Therefore, the formation of a thick zeolite supported film layer may be necessary to obtain a continuous layer made of intergrown zeolite crystals.
- A second method aims to favour nucleation processes by using a dry-gel conversion in the so-called "Vapor phase transport" method [20,21]. It is a two-step method. An amorphous gel containing silica, aluminium is first coated on the support. The crystallization occurs in a second step, the water for the hydrothermal synthesis coming as saturated vapor from the bottom of the autoclave. The template may be present either in the water or in the gel. This approach allows a strict control of the zeolite amount deposited. Also, the location and concentration of seeds is favoured. A drawback is the possibility of cracks formation in the amorphous gel layer.
- The third method, known as "Secondary Growth Synthesis" includes an initial seeding step, during which small zeolite seed crystals are deposited on top of the support. These seeds are then grown under hydrothermal zeolite synthesis conditions in order to form a continuous zeolite layer on the substrate surface. This two-step method favours the density of initial nuclei and has been widely used [22]. The choice of the seed allows determining the nature of the membrane zeolite. Seed characteristics (size, shape, concentration) can also affect the zeolite crystal orientation in the layer [23,24] which may influence the transport properties [25].

The first, single-step, strategy appears simpler but the two other methods favour the important initial stages of the membrane structuring. However, the main goal of all three is to generate a thin, defect-free zeolite layer on top of the porous support.

Some years ago [26–28], we reported on another strategy for the preparation of zeolite membranes. The idea was to grow zeolite crystals within the pores of a ceramic alumina substrate, until complete blocking of the pore by the zeolite material (Fig. 1). The result was a continuous composite zeolite–alumina membrane, obtained via the pore-plugging method. This nanocomposite membrane led to high separation factors, the separative layer being located inside the pores of the host ceramic support [26].

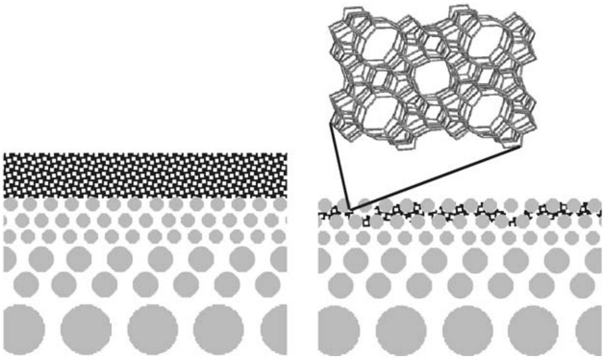

Fig. 1. Schematic comparison between film (left) and nanocomposite (right) membrane structures.

When compared to conventional zeolite toplayers grown on porous supports, the nanocomposite structure shows some potential advantages:

- In such nanocomposites, there are only discrete, small zeolite crystals, with a size in the same order as the pore diameter. Due to the intricacy of both components, when the material is submitted to large temperature changes, the thermal expansion mismatch between support and zeolite will have little effects. On the contrary, in the supported zeolite layer system, long-range stresses can build up and lead to crack formation. Such a benefit may also play a positive role during the template thermal removal, a step often considered as critical for defect-free zeolite membrane synthesis [10].
- The pore-plugging preparation route appears less challenging than the conventional methods, especially when large membrane areas are concerned. An initial imperfection will not originate a large defect, at least one not larger than the pore of the host material. This may help the scaling-up of the preparation procedure at the commercial level, with less-demanding conditions (no clean room needed).
- The separative layer is inside the porosity of the ceramic support. It is protected against abrasion and shocks. This should facilitate membrane handling and module assembling, for example when handling a catalyst in contact with the membrane for catalytic membrane reactor applications [29].

As far as we know, nanocomposite zeolite membranes have not been widely studied and only few papers describe such materials [26]. Some authors have observed such structures in parallel with conventional zeolite film growth [16]. Besides, the concept of pore plugging has been used for other membrane materials, such as Pd–ceramic composite membrane [30–32].

In this paper we mainly report on membrane synthesis and material characterization. The preparation method has been optimised using as an evaluation criterion a gas separation experiment of a mixture of adsorbing and non-adsorbing species.

Since the start of research on zeolite membrane synthesis, few authors have stressed the difficulty linked to reproducibility. This paper tries to face this problem, by dealing with many practical aspects often considered as know-how. Different parameters have been considered, such as the zeolite precursor, the hydrothermal synthesis and the host support. As a result, a new preparation method has been developed [33].

A second paper will describe gas transport properties and show how the specific nanocomposite structure of a zeolite membrane could modify permeation and separation performances.

2. Experimental

2.1. Membrane preparation

An initial standard procedure, corresponding to that used in our previous paper [26] was used as a basis for improvement. Then, starting from the first preparation step (zeolite precursor preparation) to the final one (membrane calcination), the synthesis parameters were progressively optimized. Each optimized parameter was then used in the study of the following preparation step.

However, owing to the number, complexity and intricacy of all the parameters involved in the membrane synthesis mechanisms, it was difficult to organize a proper optimization approach (i.e. analyse one experimental condition, all the other being fixed). Moreover, the probable interference of non-controlled parameters originated some scattering in the gas separation measurements. In order to minimize such effects, each precursor batch was used for two parallel preparations using the same set of conditions.

As a consequence of the above large number of parameters, added to the necessity to synthesize two samples for each conditions, a great amount of full-size tubes were prepared and all tested for defects using gas separation.

2.1.1. Zeolite precursor preparation

A clear solution was sought in order to facilitate the zeolite precursor transport inside the support pores, as needed for the pore-plugging synthesis. Aerosil 380 (Degussa) was used as silicon source, and dissolved in a 1 M tetrapropylammonium hydroxide (TPAOH, Aldrich). Note that no Al, Br or Na ions were present in these precursors. TPAOH was chosen as a structure directing agent to be sure to obtain a pure H-form membrane zeolite after calcination. The TPAOH/Si ratio was varied, the same amount of silica being put in contact with a variable amount of 1 M TPAOH. The final concentration of TPAOH was adjusted by adding deionized water to obtain a total volume of 50 ml solution, in which the Si concentration remains constant at 2 mol/l but the TPAOH concentration varies between 0.7 and 1 mol/l (providing a pH close to 14). The following overall molar proportions for the different components of the precursor solution can be given:

$$1SiO_2 : 0.35\text{–}0.5TPAOH : 27.8H_2O$$

After 3 days maturation under stirring at room temperature or 40 °C, the precursor was either used directly, or first submitted to a centrifugation step (30 min at 25 km s^{-2}), in order to remove any bulky species that might limit the precursor penetration in the support porous system.

2.1.2. Zeolite precursor characterization

In order to study the influence of the TPAOH concentration on the nature of the precursor, optical absorption and ^{29}Si NMR were used. These measurements were carried out on a Perkin-Elmer Lambda 35, in a home-made cell made of PTFE with PMMA windows, both resistant to the strongly alkaline precursor media. The transmission range of this material limited the wavelength domain to 400–900 nm.

The ^{29}Si NMR spectra were obtained on a Bruker DSX400 equipped with a solid CP-MAS probe of 7 mm diameter (no rotation, no decoupling, 4 μs pulsing time, 20 s repeat time, 2800 scans, TMS reference). The NMR acquisition was carried out during the night following the end of the maturation process.

2.1.3. Porous supports

Commercial ceramic α-alumina tubes (Pall-Exekia Membralox T1-70) were used as supports. They are made of two or three layers, of pore size decreasing from the outer to the inner side of the tube. Three support types have been used, with different average pore size for the internal top-layer. They present the following pore size sequences: 12–0.8 μm, 12–0.8–0.5 μm or 12–0.8–0.2 μm. The first 12 μm-pore layer offers a porosity of 33%, whereas that of the others is 30%. Tubes were 15 cm long, with 1 cm enamelled endings, where carbon seals can later be tighten for gas transport measurements.

Most of the optimization experiments were carried out on 0.2 μm pore size toplayer tubes, corresponding to those used in previous works [26].

Supports were characterized using a method based on gas–liquid displacement. The porous tube was first immersed in ethanol in order to fill all the porosity with liquid. An increasing pressure was then applied inside the tube in a dead-end method. According to Laplace law, the pressure for the first bubble allowed the determination of the largest passing-through pores of the support. The further increase of the permeating gas flow versus the applied pressure allowed a relative comparison of tubes of similar structure, with regards to the importance of subsequent smaller defects in the support toplayer. In the case of the 0.2 μm toplayer tubes, a reference flow rate value at 3 bar trans-membrane pressure difference, corresponding to defect diameters larger than 0.3 μm, was noted. Only supports showing a 3 bar flux lower than 1 mol/s/m^2 were used, which was the case for most of them. In order to standardize this measurement, this flow rate was taken after 5 min.

2.1.4. Hydrothermal synthesis

The stainless steel cylindrical autoclaves, designed for the shape and size of the supports (internal diameter 30 mm, depth 175 mm), were equipped with a Teflon insert covered by a Teflon cap (external diameter 29.5 mm, internal diameter 13 mm and depth 158 mm), the effective volume was ca. 21 cm^3. The zeolite precursor was poured in the autoclave containing the support until complete filling. After 10 min, some solution was added to compensate the fraction that penetrated the support, limiting the free volume in the autoclave to less than 1 cm^3.

The closed autoclave was then placed vertically in an oven preheated at 170 °C. The duration of the treatment was 4 days,

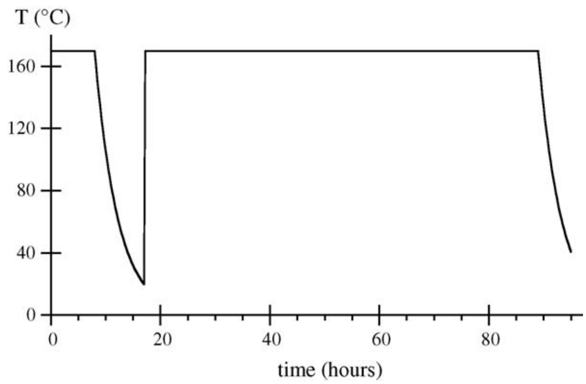

Fig. 2. Schematic of the temperature program of the hydrothermal synthesis. Temperature decrease periods are driven by the oven thermal inertia.

but the effect of an interruption was also investigated. Fig. 2 shows the oven temperature program before, during, and after the break in the hydrothermal synthesis. In some experiments the pressure in the autoclave was also measured.

After the synthesis, the tube was removed from the autoclave, washed thoroughly with deionized water, until the wash-water pH decreased below 8, and then dried at 100 °C for 12 h. Some powder was also formed outside the support tube and later calcined, weighed and characterized.

A simple N_2 permeation test was then performed to check for the presence of any open defect at this stage: the tube should be gas-tight due to the presence of the template in the pores of the zeolite crystals blocking the support pores [34]. This measurement was performed under 400 mbar differential pressure (flow detection limit 0.02 ml/min, corresponding to a permeance of ca. 10^{-10} mol m^{-2} s^{-1} Pa^{-1}).

2.1.5. Calcination procedure

The sample was placed in a glass cell, standing on a sintered porous glass disk. The template was removed by heating the sample under a stream of air or 5% O_2 in N_2. In the standard calcination procedure, the temperature was increased from room temperature to 500 °C at a rate of 1.7 °C/min, held at 500 °C for 4 h, then decreased to room temperature at a rate of 1 °C/min. In a second calcination procedure, called step calcination, the temperature was first increased at a rate of 1 °C/min to 200 °C and held at 200 °C for 2 h, then further increased at a rate of 0.5 °C/min to 500 °C and held at this temperature for 6 h, and finally decreased to room temperature at a rate of 1 °C/min.

In some cases, the tube was calcined within the gas permeation measurement module. Conditions were: 5% O_2 in N_2 at 1 ml/min in both feed and sweep sides, with no differential pressure. During the temperature increase, several N_2 permeance measurements were performed by switching the calcination gas mixture to pure N_2 and setting a differential pressure of 400 mbar. Each permeance measurement required less than 2 min, after which the calcination was carried on.

The tube weight was measured before synthesis, after the drying step and after calcination, the samples being kept under dry atmosphere.

In few cases, a complete second zeolite membrane preparation was performed after the membrane has been characterized by the gas separation experiment.

2.2. Membrane characterization

2.2.1. Gas separation measurements

Before any gas transport measurement, the membrane was first treated to remove adsorbed species, such as water coming from air humidity when the sample is exposed to atmosphere. For this cleaning procedure, the tubular membrane was mounted into the stainless steel module used for gas separation experiments. Graphite cylindrical rings (Cefilac-Fargraf) were used as seals between the membrane and the module. N_2 (20 ml/min) was introduced from both retentate and permeate sides and the module heated at a rate of 1 °C/min up to 400 °C. After a 6 h plateau, temperature was decreased to room value in ca. 3 h.

In the optimisation process, a routine test was used to follow the influence of preparation parameters on the membrane quality. This quality was evaluated using a performance measurement based on the separation of a mixture of adsorbing (*n*-butane) and non-adsorbing (hydrogen) species. As reported in [26,35,36], at low temperature, the strong adsorption of *n*-butane in the zeolite pores blocks the hydrogen permeation. In the presence of non-zeolitic crossing pores, hydrogen will permeate, even if all zeolite pores are occupied by *n*-butane molecules. Therefore, the low temperature permeate composition can be used as a very sensitive membrane quality sensor. When increasing the temperature, *n*-butane adsorption decreases and hydrogen permeation increases. This blocking effect of *n*-butane has been used to develop a simple and rapid qualitative checking method in view of industrial production testing [37].

For this separation test, a mixture of H_2 and n-C_4H_{10} diluted in N_2 (respectively, 15%, 15% and 70% in vol.) was used in Wicke-Kallenbach mode. The feed flow was 74 ml/min and the sweep flow (N_2, counter-current mode), 55 ml/min. Gas flows and feed composition were controlled by mass flow controllers (Brooks, type 5850TR and 5850E). A gas chromatograph (Shimadzu, GC-14A), using both TCD and FID detectors, measured feed, retentate and permeate compositions.

The separation factor S_f of butane over hydrogen, was calculated here as the permeate-to-feed composition ratio of the first gas, divided by the same ratio for the second one. S_f was measured at steady state and room temperature.

Pure gas permeance was not considered as an optimisation criterion, as it depends on both membrane quality (non-zeolitic defects offer preferential pathways and therefore higher fluxes) and effective thickness. As the latter cannot be easily estimated in the case of nanocomposite membranes, single-gas measurement results were taken apart. They will be treated in a future study. For information, all high-separation membranes showed pure gas (hydrogen) room temperature permeances close to 0.5 μmol/s/m^2/Pa.

2.2.2. XRD

X-Ray diffraction studies were performed using a Philips PW1050/81 diffractometer (Cu $K_{\alpha 1+2}$ radiation). Powders were obtained by scraping the inner surface of the tube with a rotating drilling machine, the weight of the sample collected was controlled. The amount obtained (≈80 mg) over 115 mm length corresponded roughly to a 20 μm depth below the inner surface of the tube.

A quantitative estimation of the composition was carried out, after calibration of peak intensities using diffractograms obtained in the very same conditions of known quantities of α-alumina and low Si/Al ratio MFI zeolite.

2.2.3. *Electron microscopy characterization*

Scanning electron microscopy (SEM) images have been obtained using a Hitachi S-800 microscope. Membrane samples have been obtained by breaking tubes in small pieces. Saw cutting was not used in order to avoid modifications in the layered structure.

Transmission electron microscopy (TEM) studies were performed with a Jeol 2010 microscope equipped for EDX analyses. Samples were prepared using a specific procedure. First, a section of the tube was cut perpendicularly to the annular plan in identical pieces. Then, the convex surface of one piece was modified to adapt to the concave surface (toplayer side) of another. The ensemble was glued and adjusted to be fixed inside a small tube of 3 mm OD. A 150 μm thick tube section was then sliced and further reduced to 20 μm by mechanical grinding with a dimpler. Finally, using ion-milling, the centre of the sample (corresponding to the toplayer location) was slimmed down till forming a small hole. TEM analyses were performed close to the hole, where the sample is thin enough for TEM material observation.

3. Results

About 100 zeolite membranes have been prepared during this optimization study. In almost all cases, the tubes were gas-tight after only one synthesis, showing the efficiency of the method used.

3.1. *Precursor characterisation*

3.1.1. *Light absorption results*

The spectra of light absorption are presented in Fig. 3.

This experiment was repeated successfully on the first solution once the four concentration values were tested. This back point on the TPAOH 1.0 mol/l precursor solution shows no deviation, showing a stable measurement system.

Fig. 3 shows a net increase of absorption (i.e. a more turbid solution) when TPAOH concentration is decreased from 1 to 0.7 mol/l. This is more specifically the case at low wavelength.

3.1.2. *NMR characterisation*

The NMR spectra obtained on similar solutions are shown in Fig. 4. These measurements were obtained with great care, and started precisely after 72 h of room temperature precursor solution maturation. However, it has to be noted that in order to obtain a reliable integration of peaks, the acquisition time (16 h) was not negligible when compared to the maturation time.

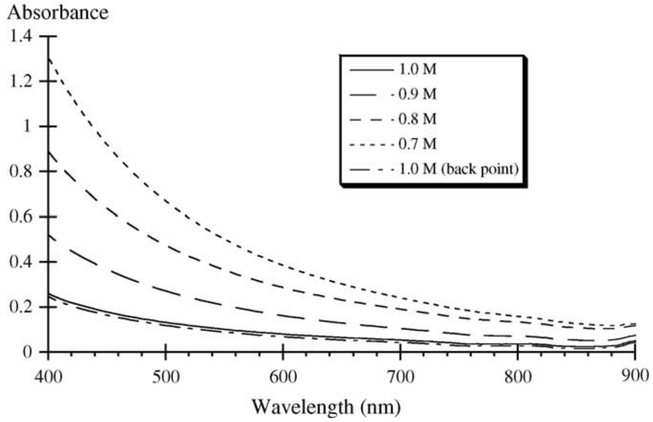

Fig. 3. Light absorption spectra of precursor solutions prepared with different TPAOH concentrations. The data are corrected for the adsorption of the cell containing only water.

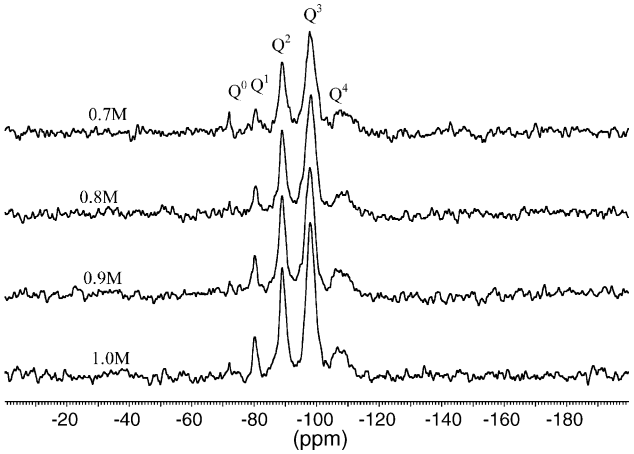

Fig. 4. NMR spectra of the different precursor solutions after maturation, showing the Q^n peaks, as a function of TPAOH concentration (from 0.7 to 1.0 mol/l).

The peaks are attributed to the different types of Si atoms in the oligomers, noted Q^n, as described in the literature [38]. The value of n, for a given Si atom, indicates the number of other Si atoms in direct connection with it through an oxygen atom bonding. This information could give some hint of oligomer size: Q^0 Si atoms are part of isolated silicate ions, Q^1 Si atoms are terminal atoms at the end of a chain, and higher n values indicate Si atoms involved in more than one Si–O–Si bond. Integrating the peaks will give a proportion of the five configurations. Table 1 gives the distribution (in %) of the integrated peaks. Note that these values are approximated, due to the signal/noise ratio.

Table 1
Distribution of peak integration values for the various Q^n

[TPAOH] (mol/l)	Q^0 (%)	Q^1 (%)	Q^2 (%)	Q^3 (%)	Q^4 (%)
0.7	2	5	24	56	12
0.8	1	5	25	60	9
0.9	2	8	29	52	10
1.0	1	6	27	57	9

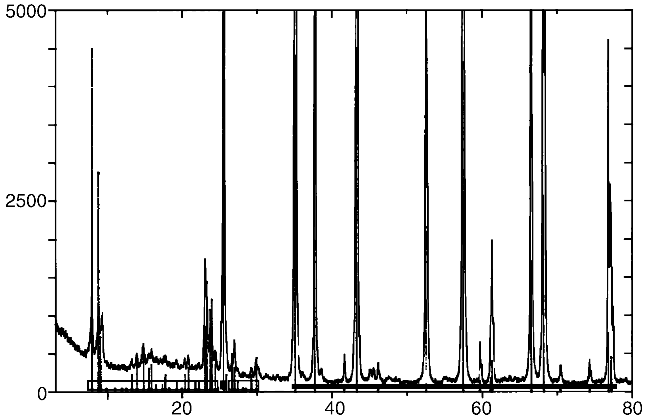

Fig. 5. Typical XRD powder diffractogram of the membrane material. The bars underlined by an open frame represent the JCPDS reference for the silicalite structure, and those underlined with a full black frame show the peaks of corundum (α-alumina).

3.2. Membrane morphology

3.2.1. XRD study

Fig. 5 shows a diffraction pattern of the powder collected from a tube after synthesis and calcination. Beside α-alumina, the other peaks correspond to the MFI structure. There is no evidence of significant presence of amorphous silica. Considering the material depth collected for analysis (≈20 μm), this diffractogram mainly shows the crystallography of the support top-layer (the 0.2 μm pore size area in this case). A quantitative estimation shows a mass ratio of MFI to alumina in the membrane scraped powder close to 9 ± 1 wt.%.

3.2.2. Electron microscopy characterization

Fig. 6 shows a scanning electron micrograph of the cross section of a tubular support (0.2 μm toplayer) after zeolite synthesis and calcination using the optimized conditions. The three layers of the support (12, 0.8 and 0.2 μm pore size, in this case) are visible. Some material is present in all the pores of the support, and can be identified as MFI crystals in the larger pores (10 μm layer) and on top of the support as poorly interconnected ones.

As it is difficult to identify the nature of the material present in the support toplayer pores on the SEM pictures, transmission electron microscopy was used further on. Fig. 7 shows micrographs, corresponding to the 0.2 μm support top-layer after zeolite synthesis. In the smaller magnification micrograph, α-Al_2O_3 corresponds to the darker areas (as shown by EDX analysis). A crystalline material (larger magnification micrograph, on the right) fills up completely the pores generated by the alumina particles. This material shows regular crystallographic intervals and fast Fourier transform method revealed the MFI zeolite structure (Fig. 7, bottom right). A similar composite material organisation has been observed on the different areas examined by this technique. No intercrystalline zeolite boundaries have been noted. Moreover, in some cases, FFT showed the same zeolite crystal orientation within neighbouring support pores (Fig. 7, top left).

EDX elemental analysis of the zeolite crystal was carried out on different spots using a probe size of about 10 nm, which allowed the selective analysis of the material present within the pores of the host alumina support. Results indicate an average Si/Al ratio of about 10 all over the MFI crystals filling the pores.

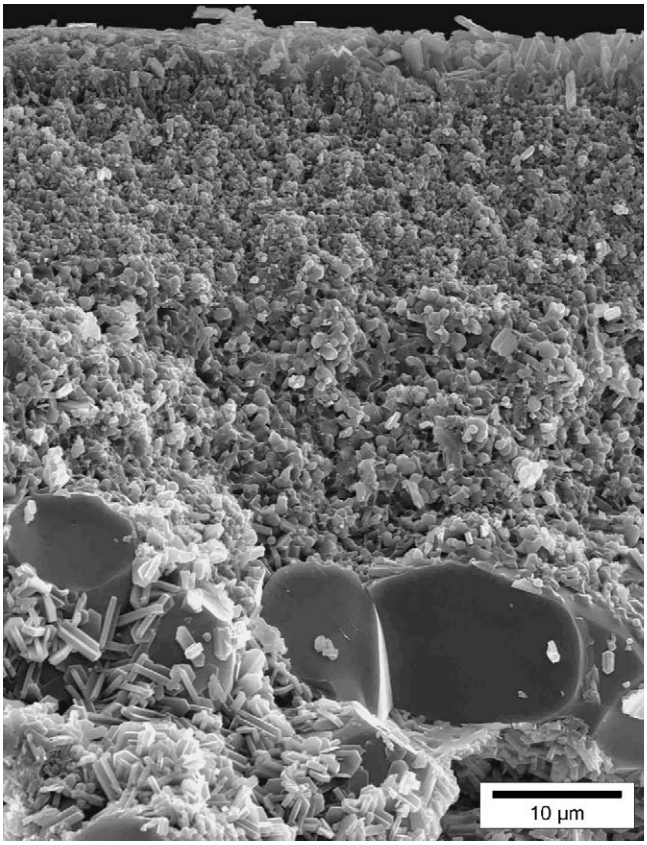

Fig. 6. Scanning electron micrograph of an alumina–zeolite nanocomposite membrane cross-section. The lower part shows the large particles of the 12 μm pore size first layer. Subsequent 0.8 and 0.2 μm pore layers can be seen upward, below a series of zeolite crystals on the top.

3.3. Membrane separative performance

3.3.1. Separation data

Fig. 8 shows typical results of hydrogen/*n*-butane separation experiments versus temperature, as obtained from two different membranes.

As previously mentioned, in the present optimization study, all prepared membranes have been compared on the basis of their room temperature separation factor, S_f (nC_4H_{10}/H_2). Membranes have been ranked in three classes according to the range of S_f values:

- Class A: $S_f > 20$
- Class B: $10 < S_f < 20$
- Class C: $S_f < 10$.

3.3.2. Zeolite precursor effect

3.3.2.1. Maturation temperature. While the main part of the samples was prepared using precursor solutions matured at room temperature, several membranes were prepared after precursor maturation at a constant temperature of 17 °C (water cooled) or 40 °C (regulated bath). No significant effect has been observed.

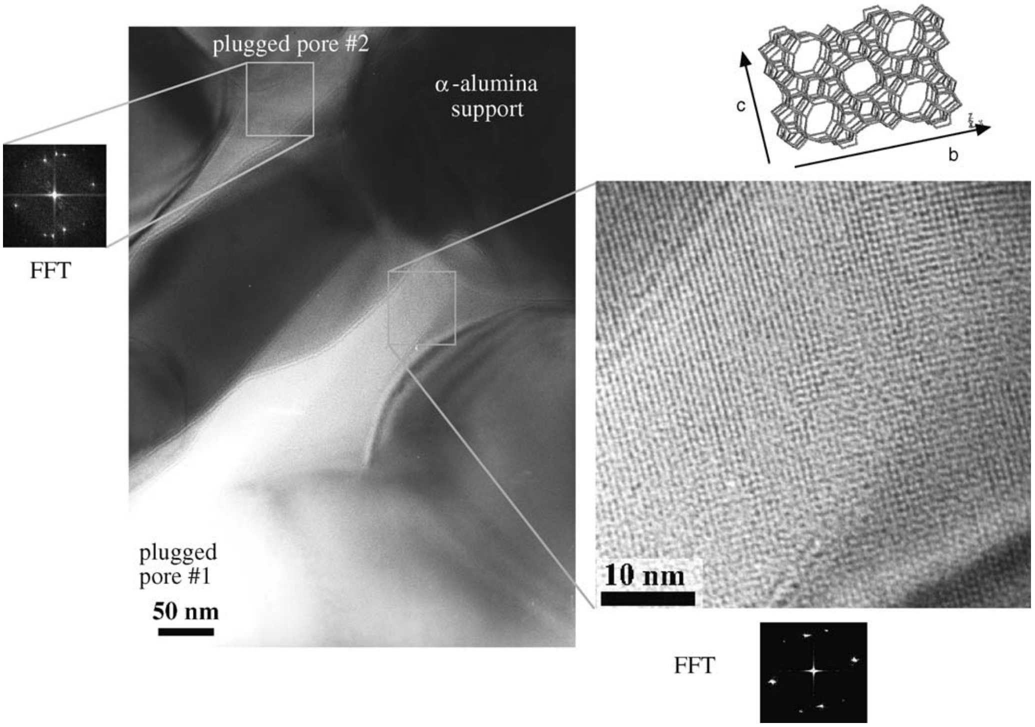

Fig. 7. Transmission electron micrograph of the zeolite/alumina composite membrane. The area shown is located inside the support top-layer (0.2 μm pore size). Right: enlargement and fast Fourier transform showing the crystal parameter analysis. Top left: similar crystal orientation in another of the support pores.

3.3.2.2. Precursor centrifugation. A positive effect has been observed. As a matter of fact, a comparative study based on 17 samples showed that the centrifugation led to an average S_f increase by a factor of 2 (without centrifugation, only class C membranes have been obtained). After centrifugation and removal of the liquid fraction, a solid residue could be collected (average weight after drying, 0.1 g).

3.3.2.3. Precursor solution composition. Using the above optimized parameters (room temperature maturation and centrifugation), the TPAOH concentration was varied. Fig. 9 gives the S_f values (as measured after membrane synthesis) according to the TPAOH concentration value in the precursor solution.

A clear maximum is observed for [TPAOH] = 0.9 mol/l, corresponding to a TPAOH/Si molar ratio of 0.45. Though the number of samples is much lower for low [TPAOH] values, it can be seen that the A/B/C classification is much better for [TPAOH] = 0.9 (65% class A, no C) than for any other value (from 50% to 100% of class C).

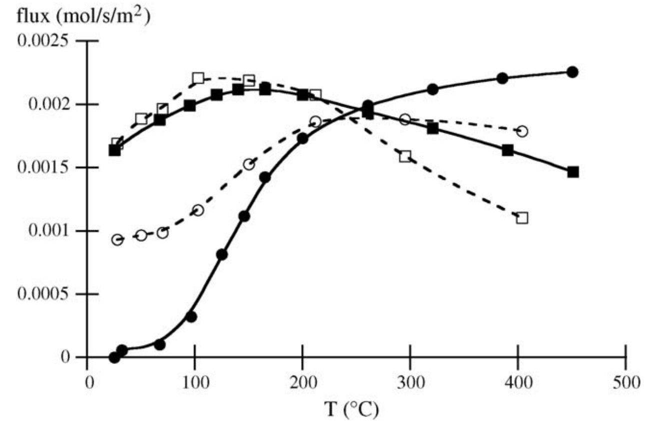

Fig. 8. Hydrogen/*n*-butane separation as a function of temperature. Squares: *n*-butane fluxes, disks: hydrogen fluxes. Black symbols: high separation membrane (room temperature $S_f = 25$), white symbols: low separation membrane ($S_f = 1.7$).

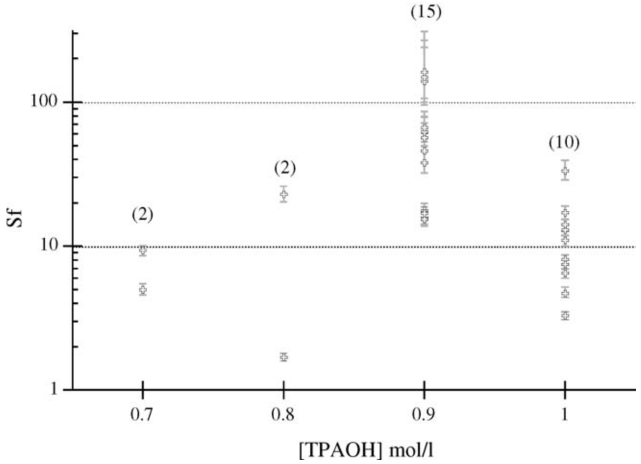

Fig. 9. Hydrogen/*n*-butane separation factors (⌖) of membranes prepared in similar conditions, apart from the TPAOH concentration in the precursor solution. The error bars (⌖) have been calculated from minima–maxima potential data. Values between brackets indicate the number of samples prepared for each condition.

According to the present results, further membrane preparations were carried out with a precursor prepared with TPAOH/Si molar ratio of 0.45, maturated at room temperature and centrifugated.

3.3.3. Hydrothermal synthesis protocol influence

3.3.3.1. Precursor introduction. In order to avoid embolismic phenomena when pouring the zeolite precursor in the autoclave containing the porous support, the ceramic tube was placed under vacuum during the precursor introduction. However, no positive effect of this parameter was observed on membrane quality.

To further reduce the autoclave free volume during hydrothermal synthesis, water was introduced in the space present between the autoclave walls and the insert. This had a clear beneficial effect, as some membranes prepared without this precaution showed very low separation factors. Too large a free volume in the autoclave would allow evaporation, followed by condensation during the synthesis break, therefore leading to a decrease of solution level, as the autoclave was positioned vertically. The tubes obtained without this precaution could have not completed zeolite synthesis in their upper part, during the second plateau of the hydrothermal synthesis.

3.3.3.2. Interruption during hydrothermal synthesis. The pressure in the autoclave was 19 bar right before the break and increased up to 27 bar during the second plateau. The interruption led to higher S_f values. In a comparative study, carried out with previously optimized conditions, and involving 25 samples, the average S_f value obtained with interruption was 60 (66% samples class A, no class C) and only 14 without interruption (no class A). The same positive effect of the break was also obtained with the original standard TPAOH/Si ratio of 0.5 (average $S_f = 11$ and 4, respectively). A longer break did not improve S_f values.

The conventional precursor introduction, with water outside the Teflon insert, and the synthesis interruption have been kept in further experiments.

3.3.4. Calcination mode influence

During calcination in the glass cell, the two-step mode did not originate any positive effect on the S_f value, when compared to the linear temperature increase.

When using the gas separation module to calcine the membranes, N_2 permeances were measured as a function of the temperature. In almost all cases, permeation started at ca. 320 °C, showing the initial membrane pore opening. This temperature was independent from the S_f performance measured later, after calcination. Using the gas permeation module for this step did not lead to an increase of the separation performance.

The simpler one-step calcination in the glass cell was selected in further membrane preparations.

3.3.5. Weight uptakes

The weight uptakes of 30 samples, as measured after the calcination step, are given, as a function of the TAPOH concentration in the precursor solution, in Fig. 10.

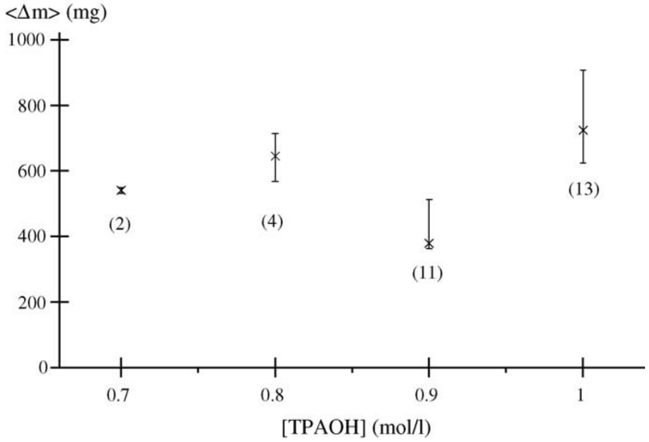

Fig. 10. Average mass uptake of zeolite membranes after calcination (×), as a function of TPAOH concentration in the precursor solution. The error bars indicate the minimum and maximum of the mass uptake for each series of comparable synthesis conditions. The number between brackets under each point gives the amount of membranes prepared for each condition.

For each concentration, the number of samples is not the same, as some synthesis conditions were given up quickly, considering the lower quality of the membrane obtained. Taking into account the powder found with the membrane in the autoclave (≈1 g of MFI as seen by XRD), the weight yield of MFI production in the membrane varied between 20% and 45%.

3.4. Support type

Using the optimized preparation method, 15 membranes have been synthesised with 0.2 μm toplayer supports. All materials were gas-tight before template removal. The average S_f value, as calculated from the separative performances of these 15 samples, is 60.

On both 0.5 and 0.8 μm toplayer supports, using the optimised preparation, no gas-tight material was obtained before template removal. At this stage, average N_2 permeances of 3 and 20×10^{-9} mol m^2 s^{-1} Pa^{-1} were obtained. After calcination, very low S_f values were obtained (between 1 and 2). A second synthesis was made on two 0.8 toplayer samples, without any progress on the observed S_f values.

4. Discussion

4.1. Material structure

The X-ray diffraction pattern (Fig. 5) shows an important proportion of MFI material in the structure of the inner part of the membrane tube (20 μm depth).

Assuming a support porosity of 30%, and taking into account the density difference between alumina and MFI, a complete MFI filling of the toplayer support pores would result in a zeolite weight fraction of about 16%. Therefore, the value obtained from XRD data (9 wt.%) indicates an important amount of zeolite inside the pore of the support. Even taking into account the contribution of the unconnected crystals that can be seen on top of the support in Fig. 6 (≈3 vol.%), one can estimate the pore filling to be above one third of the sample porous volume. This result is in agreement with previous EDX characterisations published in [26], provides a higher accuracy and confirms the pore-filling hypothesis proposed at the time.

Apart from the global characterisation provided by XRD, different electron microscopy techniques have been used for a local investigation of the composite membrane structure. Scanning electron micrographs (such as Fig. 6), show a large amount of zeolite material in the 10 μm pore support layer. Considering the weight uptake (Fig. 10), and the above estimates, the main part of the zeolite material is located in this 10 μm pore part of the support. However, this amount counts for about 20% of the total support porous volume. Therefore, the hydrodynamics properties of the support can't be much altered.

When compared to previously published scanning electron micrographs of zeolite top-layers [39], one can see in this work (Fig. 6) poorly connected zeolite crystals on the top of the support. This suggests that the separation capabilities are not provided by these crystals. Therefore, the separative layer is likely made of a continuous composite MFI/alumina matrix located within the 0.8 and/or 0.2 μm pore layers of the support tube. Looking more closely to this structure by TEM (Fig. 7), zeolite crystals, filling up completely the support porous volume, were identified. The alumina/zeolite interface is continuous.

The fact that there is no grain boundaries visible in the whole area investigated by TEM does not mean they are not present. However, this suggests that they are not statistically significant. As a consequence, the transfer through the membrane should be controlled by zeolite pores and not by grain boundaries.

Another information provided by TEM is a very low Si/Al ratio of the MFI crystals grown into the alumina matrix. Considering the precursor solution was Al-free, this element must have been extracted, from the tube wall material, by the very alkaline media during synthesis. Moreover, elemental analysis of the MFI powder produced during the same synthesis outside the support gave very high Si/Al values (over 600), and the mother liquor contained no Al. Therefore, the Al extraction process is very localised to the inside of the support pores, as observed by Sasaki et al. [16]. This shows that, during the hydrothermal synthesis, the Al extraction rate is lower than that of its insertion into the growing MFI crystal.

On larger pore size support (0.5 and 0.8 μm toplayers), the pore plugging is not complete as observed from the results presented in Section 3.4 (no gas separation). There seems to be a critical support pore diameter above which crystallisation inside the pore does not plug it totally. As the pore sizes mentioned above are average, this critical value should be higher than 0.5 μm. Fig. 6 shows that MFI zeolite crystals synthesised without wall constraint inside or in contact with the support structure reach a maximum size of 5 μm × 1 μm. One can imagine that in the distribution of crystal sizes and pore size may result in some pores unplugged, when the average support pore size is 0.5 μm or above. Besides this distribution of crystal size may be shifted toward smaller size when growth is inhibited in confined conditions. Moreover, assuming a similar nuclei surface density during synthesis, the large difference of porous surface/volume ratios may help explaining the unplugging of larger support pores.

On the other hand, the pore size distribution on 0.2 μm toplayers might be responsible for the discrepancy of separation ability obtained, taking into account this limitation of pore plugging in larger pores.

4.2. Synthesis conditions and membrane performance

As previously introduced, *n*-butane/hydrogen separation has been used as optimisation criterion for membrane performance. The idea of using a mixture of adsorbing (*n*-butane) and non-adsorbing (hydrogen) species to assess the membrane quality seems well adapted to zeolite materials. As a matter of fact, microporous non-zeolitic defects may inhibit this adsorption-based separation. Moreover, if Knudsen-type defects exist, they will favour the transport of the lighter species, i.e. hydrogen. This will strongly decrease the experimental S_f value, as hydrogen is the mixture component that is blocked by *n*-butane strongly adsorbed within the zeolite pores.

Other separation tests [40], such as molecular sieving-based separations (SF_6/N_2, for example), or diffusion-based separations (such as normal/isobutane) could not be as discriminative, considering Knudsen-type defects will either show some separative efficiency (in the case of SF_6/N_2), or be neutral (*n*/isobutane).

Fig. 9, showing the influence of TPAOH concentration on membrane quality (S_f), reveals a clear maximum for 0.9 mol/l, all other conditions being equal. Even if it is true that 0.7 and 0.8 mol/l conditions offer less samples than the other two, the trend is similar if all samples prepared, including variations in other experimental conditions, are taken into account. Let us consider the different aspects that may lead to such an influence.

4.2.1. Zeolite precursor effect

Characterisations of the precursor solutions before synthesis do not correspond exactly to the situation during hydrothermal synthesis, but they can give some insight about the precursor state at the start of the synthesis. Fig. 3, giving the light absorption of the solutions, indicates smaller particles are present when TPAOH concentration increases from 0.7 to 1.0 mol/l. The decrease of the absorbance when increasing the wavelength also suggests more small particles than large ones that are present. After centrifugation the precursor solution turns clear, showing that all these large particles have been removed. However, this size distribution trend, as a function of the TPAOH concentration, should be similar with the smaller oligomers remaining in suspension after centrifugation, and used during hydrothermal synthesis. NMR analysis (Fig. 4 and Table 1) has been performed in order to characterize the precursor at a smaller scale. It shows there is no clear difference between the silicon atomic environments in the precursor species. However, there might be differences at the colloidal scale, as can be assumed considering the light adsorption data. This matter could be studied using other techniques that are not easily accessible [38].

4.2.2. *Hydrothermal synthesis in alumina pores*

The description of nucleation and crystal growth is complex [41,42]. In this work, the situation is even more difficult to describe in details, due to the presence of the alumina support, dissolving during synthesis. This aluminium may affect both nucleation and crystal growth steps [16]. Moreover, precursor transport within the pores could play an important role.

As suggested by light absorption experiments (Fig. 3), an increase of TPAOH concentration leads to smaller precursor species in suspension, which may favour their transport within the pores and hence the pore-plugging process. This factor may be counterbalanced when too high a TPAOH concentration would extract too much aluminium, leading to a limitation of the crystal growth in the support pores [41]. These two antagonist influences may originate an optimum for the efficiency of the pore plugging synthesis. In agreement with this hypothesis, a parallel optimum in the membrane quality, as observed on separation factor data (Fig. 9), can occur for an intermediate value of TPAOH concentration.

The interruption of the hydrothermal synthesis shows a statistic positive effect, as mentioned in Section 3.3.3. The zeolite synthesis generates relatively large amounts of gaseous species when compared to the autoclave free volume. Therefore, the pressure evolution before and after the interruption shows that the MFI formation is not completed at this point. One can assume that the first temperature period corresponds to a germination step. Later on, the cut in the synthesis process could favour the transport of fresh precursor into the support pores during the period when no precursor is consumed. This process may favour an efficient pore-plugging. One can expect that without this interruption, the zeolite crystallisation would mainly occur on the outside surface of the support toplayer or at the mouth of its pores, leading to a hindrance of precursor transport inside them. Therefore, the pore plugging probability would be decreased, leading to poorer separative performances.

5. Conclusion

The pore-plugging synthesis of nanocomposite MFI-alumina membranes has been optimised with regards to a series of parameters. Among these, the composition of the precursor solution and the support pore size showed a strong influence on the final membrane quality. Moreover, the introduction of an interruption during the hydrothermal synthesis led to higher membrane separative performances. Whilst the effect of the first two has been thoroughly investigated, the influence of this break is still under scrutiny.

The nanocomposite structure of the membrane has been studied at both macroscopic and microscopic scales. A continuous MFI-alumina configuration has been observed. In this specific design, grain boundaries, if any, do not seem to affect transport through the membrane. This material architecture may modify the transport and separation properties in comparison with supported zeolite films. These aspects will be dealt with in a future paper. Moreover, as suggested from the calcination results, this material structure provides a high tolerance to thermal stress. This is probably due to the absence of the long-range stress that can observed in supported zeolite films [43–45].

These nanocomposite membranes have been extensively used for different applications. In xylene isomer separation [46] and ammonia recovery [47] this material has shown interesting performances. Moreover, it has been successfully combined with catalyst for isobutene dehydrogenation [48], and xylene isomerization [46]. In these applications, the nanocomposite alumina/zeolite membrane showed high thermal and mechanical resistance.

Acknowledgements

Olga Pachtová Prokopová expresses all thanks to the Grant Agency of the Czech Republic for the Grant No. 104/03/D183 and to the Region Rhône-Alpes for the Tempra/Peco program 2000. Yu Sun acknowledges the French Minister for Research and Technology for his post-doc grant. Yong Sheng Li is grateful to the CNRS for his associate researcher grant. The European Union is kindly acknowledged for granting projects CT95 0018 “Microporous ceramic membranes for gas separation processes” and G1RD-CT1999-00078 “Improved membranes and processes for the low energy recovery of ammonia in synthesis plants” (Impress). The authors would like to thank the Institut Français du Pétrole and the Société des Céramiques Techniques (now Pall-Exekia) for financial and technical supports.

The authors would like to give special thanks to Alain Tuel, Valentin Valtchev and Milan Kocirik for fruitful discussion about zeolite synthesis. They are grateful to Chantal Lorentz for the results obtained on the NMR facility at CNRS/IRC.

References

[1] Y. Morigami, M. Kondo, J. Abe, H. Kita, K. Okamoto, The first large-scale pervaporation plant using tubular-type module with zeolite NaA membrane, Sep. Purif. Technol. 25 (2001) 251.

[2] S. Tennison, Current hurdles in the commercial development of inorganic membrane reactors, Membr. Technol. 2000 (2000) 4.

[3] C.E. Marshall, The use of zeolitic membrane electrodes, J. Phys. Chem. 43 (1939) 1155.

[4] M.J. Den Exter, J.C. Jansen, J.M. Van De Graff, F. Kapteijn, J.A. Moulijn, H. Van Bekkum, Zeolite-based membranes preparation, performance and prospects, Stud. Surf. Sci. Catal. 102 (1996) 413.

[5] M. Matsukata, E. Kikuchi, Zeolitic membranes: synthesis, properties, and prospects, Bull. Chem. Soc. Jpn. 70 (1997) 2341.

[6] F. Mizukami, Application of zeolite membranes, films and coatings, Stud. Surf. Sci. Catal. 125 (1999) 1 (porous materials in environmentally friendly processes).

[7] J. Coronas, J. Santamaría, Separations using zeolite membranes, Sep. Purif. Methods 28 (1999) 127.

[8] A. Tavolaro, E. Drioli, Zeolite membranes, Adv. Mater. 11 (1999) 975.

[9] J.D.F. Ramsay, S. Kallus, in: N.K. Kanellopoulos (Ed.), Recent Advances in Gas Separation by Microporous Ceramic Membranes, vol. 6, Elsevier, 2000, p. 373.

[10] Y.S. Lin, I. Kumakiri, B.N. Nair, H. Alsyouri, Microporous inorganic membranes, Sep. Purif. Methods 32 (2002) 229.

[11] M. Noack, J. Caro, in: F. Schueth, K.S.W. Sing, J. Weitkamp (Eds.), Handbook of Porous Solids, vol. 4, Wiley-VCH Verlag GmbH & Co., Weinheim, Germany, 2002, p. 2433.

[12] S. Nair, M. Tsapatsis, in: S.M. Auerbach, K.A. Carrado, P.K. Dutta (Eds.), Handbook of Zeolite Science and Technology, Marcel Dekker, Inc., New York, 2003, p. 867.

[13] T.C. Bowen, R.D. Noble, J.L. Falconer, Fundamentals and applications of pervaporation through zeolite membranes, J. Membr. Sci. 245 (2004) 1.

[14] A. Julbe, Zeolite membranes—a short overview, Stud. Surf. Sci. Catal. 157 (2005) 135.

[15] T. Bein, Synthesis and applications of molecular sieve layers and membranes, Chem. Mater. 8 (1997) 1636.

[16] Y. Sasaki, W. Shimizu, Y. Ando, H. Saka, Microstructure analysis with TEM for zeolite layer formed in pore of porous alumina substrate, Microporous Mesoporous Mater. 40 (2000) 63.

[17] I. Kumakiri, T. Yamaguchi, S.-I. Nakao, Preparation of zeolite a and Faujasite membranes from a clear solution, Ind. Eng. Chem. Res. 38 (1999) 4682.

[18] J. Caro, M. Noack, P. Kölsch, R. Schäfer, Zeolite membranes—state of their development and perspective, Microporous Mesoporous Mater. 38 (2000) 3.

[19] S.P. Davis, E.V.R. Borgstedt, S.L. Suib, Growth of zeolite crystallites and coatings on metal surfaces, Chem. Mater. 2 (1990) 712.

[20] W. Xu, J. Dong, J. Li, J. Li, F. Wu, A novel method for the preparation of zeolite ZSM-5, J. Chem. Soc., Chem. Commun. 10 (1990) 755.

[21] T. Matsufuji, N. Nishiyama, M. Matsukata, K. Ueyama, Separation of butane and xylene isomers with MFI-type zeolitic membrane synthesized by a vapor-phase transport method, J. Membr. Sci. 178 (2000) 25.

[22] G. Bonilla, D.G. Vlachos, M. Tsapatsis, Simulations and experiments on the growth and microstructure of zeolite MFI films and membranes made by secondary growth, Microporous Mesoporous Mater. 42 (2001) 191.

[23] A. Gouzinis, M. Tsapatsis, On the preferred orientation and microstructural manipulation of molecular sieve films prepared by secondary growth, Chem. Mater. 10 (1998) 2497.

[24] J. Hedlund, M. Noack, P. Kolsch, D. Creaser, J. Caro, J. Sterte, ZSM-5 membranes synthesized without organic templates using a seeding technique, J. Membr. Sci. 159 (1999) 263.

[25] Z. Lai, G. Bonilla, I. Diaz, J.G. Nery, K. Sujaoti, M.A. Amat, E. Kokkoli, O. Terasak, R.W. Thompson, M. Tsapatsis, D.G. Vlachos, Microstructural optimization of a zeolite membrane for organic vapor separation, Science 300 (2003) 456.

[26] A. Giroir-Fendler, J. Peureux, H. Mozzanega, J.-A. Dalmon, Characterisation of a zeolite membrane for catalytic membrane reactor application, Stud. Surf. Sci. Catal. 101A (1996) 127.

[27] J. Ramsay, A. Giroir-Fendler, A. Julbe, J.-A. Dalmon, Matériau inorganique poreux, notament sous forme de membrane, et procédé d'obtention d'un tel matériau, France Patent 9405562 (January 7, 1994).

[28] D. Uzio, J. Peureux, A. Giroir-Fendler, J.-A. Dalmon, J.D.F. Ramsay, Formation and pore structure of zeolite membranes, Stud. Surf. Sci. Catal. 87 (1994) 411.

[29] S. Miachon, J.-A. Dalmon, Catalysis in membrane reactors: what about the catalyst? Top. Catal. 29 (2004) 59.

[30] K. Kusakabe, S. Yokoyama, S. Morooka, J.-I. Hayashi, H. Nagata, Development of supported thin palladium membrane and application to enhancement of propane aromatization on Ga–silicate catalyst, Chem. Eng. Sci. 51 (1996) 3027.

[31] S. Miachon, A. Mazuy, J.-A. Dalmon, Catalysis of palladium salt reduction in a gas–liquid membrane reactor, Stud. Surf. Sci. Catal. 130 (2000) 2693.

[32] G. Xomeritakis, Y.S. Lin, Fabrication of a thin palladium membrane supported in a porous ceramic substrate by chemical vapor deposition, J. Membr. Sci. 120 (1996) 261.

[33] C. Chau, I. Prévost, S. Miachon, J.-A. Dalmon, Process for preparing supported zeolitic membranes by temperature-controlled crystallisation, US Patent 6,582,495 (June 24, 2003).

[34] R.D. Noble, J.L. Falconer, Silicalite-1 zeolite composite membranes, Catal. Today 25 (1995) 209.

[35] F. Kapteijn, W.J.W. Bakker, J.V.D. Graaf, G. Zheng, J. Poppe, J.A. Moulijn, Permeation behaviour of a silicate-1 membrane, Catal. Today 25 (1995) 213.

[36] M. Yang, B.D. Crittenden, S.P. Perera, H. Moueddeb, J.A. Dalmon, The hindering effect of adsorbed components on the permeation of a non-adsorbing component through a microporous silicalite membrane: the potential barrier theory, J. Membr. Sci. 156 (1999) 1.

[37] O. Pachtová, I. Kumakiri, M. Kocirik, S. Miachon, J.-A. Dalmon, Dynamic desorption of adsorbing species under cross membrane pressure difference: a new defect characterisation approach in zeolite membranes, J. Membr. Sci. 226 (2003) 101.

[38] C.J.Y. Houssin, C.E.A. Kirschhock, P.C.M.M. Magusin, B.L. Mojet, P.J. Grobet, P.A. Jacobs, J.A. Martens, R.A.V. Santen, Combined in situ 29Si NMR and small-angle X-ray scattering study of precursors in MFI zeolite formation from silicic acid in TPAOH solutions, PCCP 5 (2003) 3518–3524.

[39] J. Hedlund, J. Sterte, M. Anthonis, A.-J. Bons, B. Carstensen, N. Corcoran, D. Cox, H. Deckman, W.D. Gijnst, P.-P.D. Moor, F. Lai, J. McHenry, W. Mortier, J. Reinoso, J. Peters, High-flux MFI membranes, Microporous Mesoporous Mater. 52 (2002) 179.

[40] M. Noack, P. Kölsch, R. Schäfer, P. Toussaint, J. Caro, Molecular sieve membranes for industrial application: problems, progress, solutions, Chem. Eng. Technol. 25 (2002) 221.

[41] C.S. Cundy, P.A. Cox, The hydrothermal synthesis of zeolites: precursors, intermediates and reaction mechanism, Microporous Mesoporous Mater. 82 (2005) 1.

[42] V.P. Valtchev, K.N. Bozhilov, Evidences for zeolite nucleation at the solid-liquid interface of gel cavities, J. Am. Chem. Soc. 127 (2005) 16171.

[43] J. Dong, Y.S. Lin, M.Z.-C. Hu, R.A. Peascoe, E.A. Paysant, Template-removal-associated microstructural development of porous-ceramic-supported MFI zeolite membranes, Microporous Mesoporous Mater. (2000) 241–253.

[44] J. Hedlund, F. Jareman, A.-J. Bons, M. Anthonis, A masking technique for high quality MFI membranes, J. Membr. Sci. 222 (2003) 163.

[45] S. Heng, P.P.S. Lau, K.L. Yeung, M. Djafer, J.-C. Schrotter, Low-temperature ozone treatment for organic template removal from zeolite membrane, J. Membr. Sci. 243 (2004) 69.

[46] L. van Dyk, L. Lorenzen, S. Miachon, J.-A. Dalmon, Xylene isomerization in an extractor type catalytic membrane reactor, Catal. Today 104 (2005) 274.

[47] O. Camus, S. Perera, B. Crittenden, Y.C.V. Delft, F. Dick, P. Meyerb, P.A.C.Pex, I. Kumakiri, S. Miachon, J.-A. Dalmon, S. Tennison, P. Chanaud, Ceramic membranes for ammonia recovery, AIChE J., in press.

[48] P. Ciavarella, D. Casanave, H. Moueddeb, S. Miachon, K. Fiaty, J.-A. Dalmon, Isobutane dehydrogenation in a membrane reactor. Influence of the operating conditions on the performance, Catal. Today 67 (2001) 177.